Study of the phase dependency of RF cavities on gamma ray distribution

G. R. Montoya-Soto*, G. H. I. Maury-Cuna, and V. M. Lizarraga-Rubio
Departamento de Física, Universidad de Guanajuato, León 37150, México,
e-mail: gr.montoyasoto@ugto.mx

C. A. Valerio-Lizarraga, S. Millan-Estrada, C. Duarte-Galvan, C. Aguilar, I. Leon Monzon, and J. E. Leyva-Cervantes
Universidad Autónoma de Sinaloa, Culiacán 80000, México.

Received 4 December 2024; accepted 30 May 2025

A front-to-end simulation study of a gamma irradiator was conducted, covering the entire process from the electron gun to the gamma rays going into a collimator, to investigate the impact of the RF phase on the irradiation process for continuous wave (CW) beams. Instead of considering an ideal monoenergetic beam to generate the gamma rays, we use a more complex simulation where initially, the electron gun generates a continuous beam of 50 keV $\pm$ 2.5 keV energy, which then passes through a multi-cell S-band RF cavity, accelerating the electrons to a final average energy of 6 MeV. Subsequently, the beam interacts with a tungsten plate downstream, generating gamma rays. An integrated simulation system consisting of specialized software for different study aspects has been developed. Poisson Superfish and CST Studio were used for RF cavity design, Travel for beam dynamics analysis, and Geant4 for simulating electron-gamma conversion and tracking. All beam properties were exported between codes in such a way that the particles position, energy, and RF phase dependency were preserved throughout. This work aims to define the realistic limits of the electron beam quality in RF electron linear accelerators for gamma irradiation.

Keywords: Electron-beam; gamma-rays; irradiation; beam dynamics; RF phase.

DOI: https://doi.org/10.31349/RevMexFis.71.051203

1. Introduction

In various applications, irradiators take a continuous low-energy electron beam and accelerate it to energies on the order of MeV using an RF cavity. However, this continuous beam cannot be fully transmitted due to the cavity's limited longitudinal acceptance capacity. Electrons that are not captured are mostly lost to the cavity walls or are decelerated. Our focus is on the electrons that successfully travel through the linear accelerator (Linac).

Several other works have studied how to improve the quality of the gamma beam produced by the Linac using a combination of collimators, and flattening filters, however, these studies have not considered the quality of the electron beam in their analysis [1-3].

In this work, we designed a compact electron Linac utilizing a (7+6)-cell S-band RF cavity operating in the $\pi/2$ mode. The design considered factors such as energy gain, energy spread, emittance evolution, and particle transmission. The S-band frequency is widely employed in accelerator applications due to its balance between maximum beam intensity and size, making it particularly suitable for a range of scientific and medical applications. Our project involved comprehensive beam dynamics simulations to assess the behavior of an electron beam as it is accelerated through the cavity.

In applications requiring small energy dispersion, a dipole is used to remove electrons with undesired energies before the collision with the target. However, the magnet is not employed in many other applications where the energy dispersion is not critical. In this study, we assume the dipole is absent and evaluate its necessity by comparing a realistic beam with an ideal mono-energetic beam. This is all done to see the feasibility of using this kind of layout in medical applications, such as breast cancer treatment.

In our layout, the electron beam is accelerated by an RF cavity. Then, it travels freely for 1 cm before colliding with a tungsten target, producing a gamma-ray shower. The gamma-ray beam is then propagated until collimation using a square-shaped iris. The collimator shape is kept as simple as possible to preserve the influence of the properties of the electron beam on the ones from the gamma-ray. This collimation serves the purpose of limiting its energy spread and transverse beam size. Finally, a water volume is placed at the end of the layout to facilitate measurements of energy deposition in the region. A figure of the layout is shown in Fig. 1.

2. RF cavity

The RF cavity was designed using Poisson Superfish [4] and CST Studio (CST) [5]. The initial section of the Linac accounts for beam velocity to improve beam transmission by employing the half-cell length approach [6]. To preserve good emittance, the cavity design constrains the transverse beam size to below 1.5 mm [6].

The electromagnetic field map of the cavity was exported to the Travel code [7] for beam dynamics simulations. An electron beam with an energy of 50 keV $\pm$ 2.5 keV and an r.m.s. size of 1 mm was used as the input beam for the cavity.

The beam particle distribution in the phase-energy plane (longitudinal plane) after passing through the cavity is shown

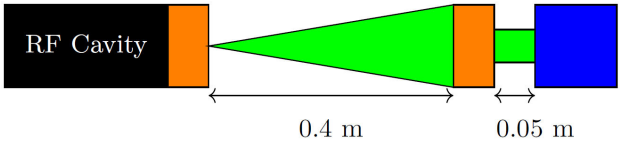

FIGURE 1. System layout. From left to right, the RF Cavity (black), the target (orange), the gamma beam (green), the collimator (orange), and the water volume (blue).

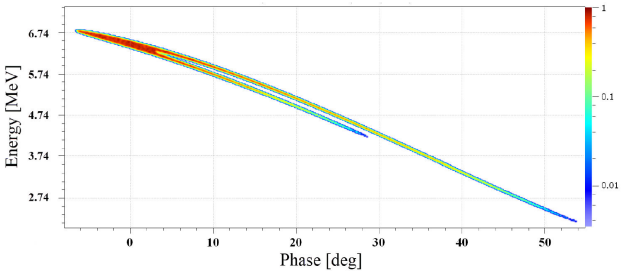

FIGURE 2. Energy phase space spectrum of the electron beam at the output of the RF cavity before colliding on the target.

in Fig. 2. The color scale represents the density of particles in a logarithmic scale. 85 % of the particles range in energy from 5.75 MeV to 6.8 MeV and in phase from -7 to 10 degrees. The beam is bunched in an optimal phase but presents a long tail of particles with a final kinetic energy below the ideal one. This indicates that, while a portion of the beam is properly accelerated, a significant number of particles, 15 % of the population, are not reaching the optimal energy due to the longitudinal acceptance of the cavity. This is the standard way of representing the beam's longitudinal phase space, and it is useful for synchronizing the cavity output with the next part of the accelerator [8,9], while being readily verifiable through energy- and time-based phase space measurements. However, one of its disadvantages is the loss of information about the particle injection phase since there is a shift in their RF phase as they travel along the cavity.

Thus, to perform an end-to-end simulation, the injection phase information of the particles must be preserved as they traverse the cavity. This ensures the ability to study the dependency of the final electron energy on the input RF phase, resulting in an energy-phase space diagram that clearly illustrates the relationship between the input phase and the final energy of the electrons. This can be seen in Fig. 3. The color scale, presented in arbitrary units, indicates the particle density, with yellow regions representing higher particle densities. The results show that particles within the phase range of -50 to 40 degrees are effectively accelerated.

From this new phase space diagram, it becomes evident how the final energy follows the RF phase. The maximum energy is achieved when the electrons enter the cavity at an input phase equal to -12 degrees. Additionally, the longitudinal capture range, where electrons can be effectively accelerated, spans from -50 to 60 degrees.

After identifying the output beam characteristics as a function of the RF input phase, a phase scan was performed to analyze the temporal evolution of all beam parameters. This

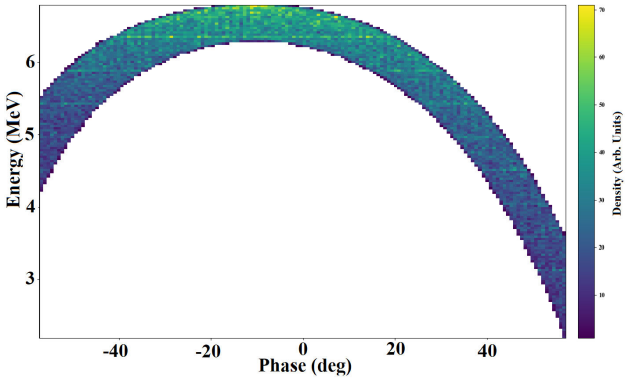

FIGURE 3. Output beam energy phase space related to the linac input RF phase.

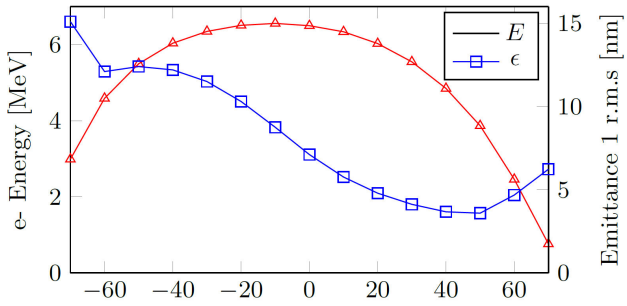

FIGURE 4. Energy and emittance dependency of the RF phase.

analysis provided insights into the evolution of emittance and average energy, revealing that the lowest emittance, observed at 50 degrees, does not align with the phase of maximum acceleration, which occurs at -12 degrees. Furthermore, the results indicate two distinct emittance values for the same energy, as shown in Fig. 4. This variability in emittance at a given energy could result in differences in the focal point when the electron beam is focused using a magnet.

Figure 4 also shows that the energy plateau ranges from -40 to 25 degrees, this allows us to set the limits for applications where beam energy dispersion is important, and where a magnet or pulsed gun would need to be added [10,11].

3. Gamma conversion

Once the electron beam passes through the cavity, it collides with a tungsten plate, generating gamma rays. To study these effects, the output beam from the cavity was exported to Geant4 [12].

The Geant4 simulation is configured with a tungsten plate positioned precisely at the output of the RF cavity, at a distance of 1 cm. At this point, the electron beam collides with the 0.4 mm thick tungsten plate, producing gamma rays through the bremsstrahlung interaction process

The target thickness has been chosen to produce gamma rays effectively [13]. Its placement is as close to the cavity as possible to minimize the dependency on the output beam

focal point. However, this configuration is known to generate back-scattered radiation, which will be neglected in this work.

Once the gamma rays are produced, they travel a distance of 0.4 m in a straight path before reaching a tungsten collimator. This collimator has dimensions of 0.1×0.1 m and a thickness of 4 cm. To monitor the evolution of the gamma beam, gamma-ray particle data is collected in three different positions: the downstream surface of the tungsten plate, right before and after the collimator. This setup enables the observation of collimation effects on beam quality, which is critical for various applications that depend on uniform irradiation. Some electrons may pass through the collimator; this phenomenon, known as 'electron contamination', has been excluded in this study.

In addition to shaping the gamma beam with the collimator, further processing can be applied to enhance its uniformity [3,14,15]. However, our focus is on preserving as much information as possible related to the beam's source. Excessive hard cuts in the beam profile may lead to a loss of critical data derived from these source-based differences.

To evaluate the generation of gamma rays of a realistic beam, such as the one shown in Fig. 2, an ideal beam was used for reference. The ideal beam has a kinetic energy of 6 MeV (with no energy dispersion), is cylindrically symmetric, and has a uniform radial distribution with a radius of 1 mm. In Fig. 5, it is shown that in both cases, 80 % of the gamma beam has an energy below 1 MeV. Additionally, the gamma beam energy distribution is observed to be identical for the two cases studied. The energy spectrum indicates that, as expected, only a small fraction of the gamma rays retain the maximum e-beam energy. This suggests that the gamma beam properties like the energy dispersion, and emittance are dominated by the target thickness, as summarized in Table I.

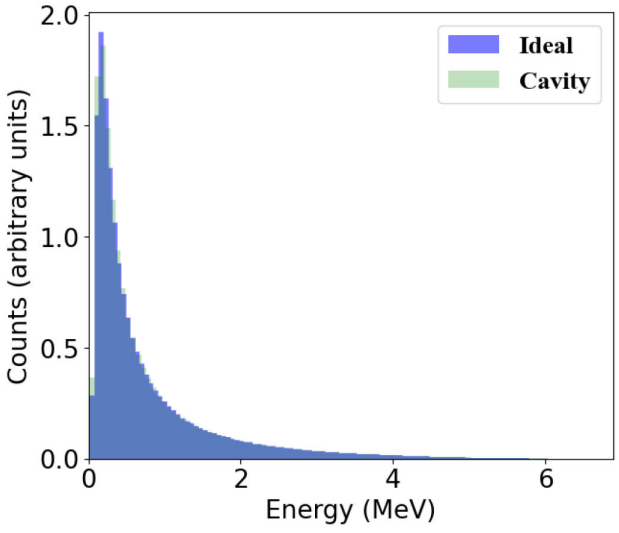

FIGURE 5. Gamma beam energy spectrum at the collimator entrance with the beam generated using an ideal beam and the RF cavity output from Fig. 2.

TABLE I. Gamma beam parameters after target collision.

Parameter	Ideal	Realistic
Emittance (m.rad)	0.06	0.05
Mean Energy (MeV)	0.99	0.95
Energy Disp. (MeV)	1.02	0.99

The emittance values are similar, but the reason why the real beam has a lower emittance can be attributed to the cavity giving a profile similar to a Gaussian distribution, while the ideal beam follows a uniform distribution.

4. Gamma beam and RF phase effect

Using the two extreme cases of the electron beam properties presented in the previous section, we compared the effect of the RF phase on the gamma beam after the tungsten target. Figure 6a) shows that the mean energy of the produced gamma beam follows a similar trend to that of the electron beam, providing insight into the overall dependency of beam quality. It is observed that the gamma beam energy never exceeds 17 % of the electron beam energy within the RF phase range of -70 to 50 degrees.

It is presented in Fig. 6b) that the gamma beam emittance and energy spread do not share the same trend. This discrepancy holds within the constraints of the beam dispersion given by the RF cavity, whereas the electron-gamma conversion, within the target, dominates the gamma beam quality.

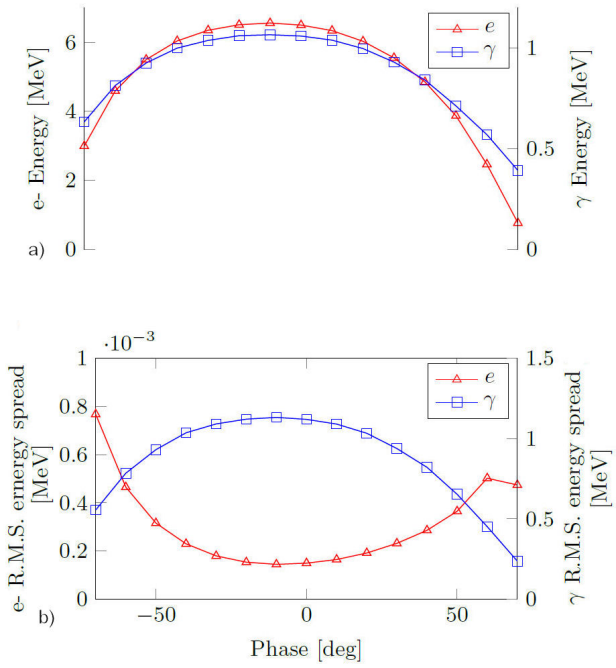

FIGURE 6. Average energy a) and energy spread b) at the RF cavity output for electrons, and immediately after the tungsten target for gamma rays.

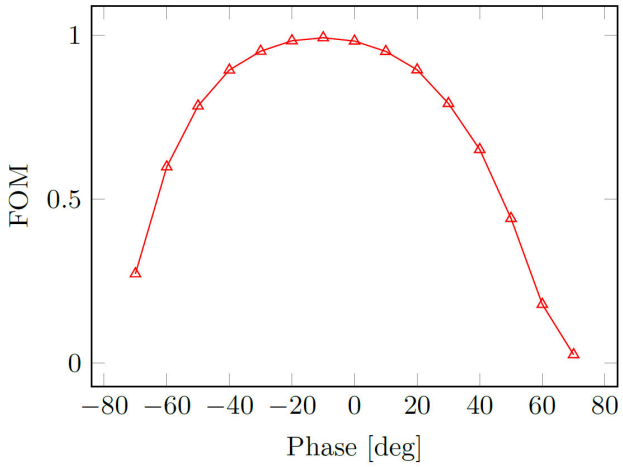

FIGURE 7. FOM of the gamma beam power right after the target.

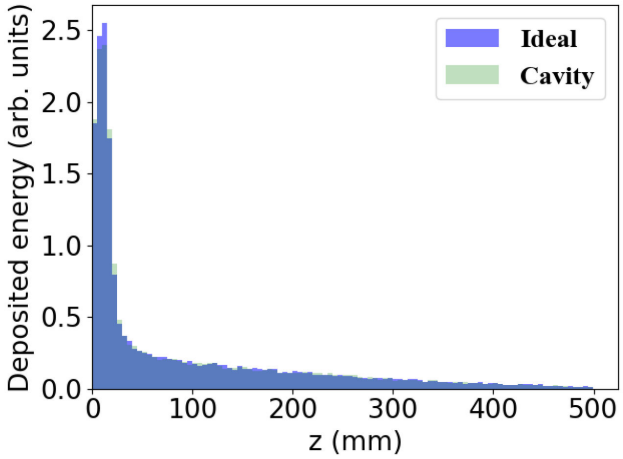

FIGURE 8. Profile of the gamma rays energy deposition in a water volume for the monoenergetic and cavity beam.

We define a figure of merit (FOM) for the gamma beam power, calculated as the product of the gamma beam's mean energy, E_γ, and the conversion efficiency, η. Figure 7 illustrates the correlation between the FOM and the optimal phase, showing that the beam power decreases to below 60% beyond the 50-degree phase window.

The inclusion of a dipole magnet after the cavity will allow us to select the electron beam energy that can be seen as a selection window on the RF phase from Fig. 3 proportional to the beam bending angle, as the bending angle increases, the beam will tend to the monoenergetic beam previously studied.

5. Deposited energy comparison

The most important parameter for the user of a gamma irradiator is to assess how uniformly a volume can be irradiated. To complete our study we compare the deposited energy in a water volume from the gamma rays created by the ideal monoenergetic and the realistic beam from the RF cavity.

The energy deposited by gamma rays was monitored in a water volume sectioned longitudinally, allowing for precise tracking of the energy distribution across different regions of the sample. When the gamma rays interacted with the water volume, the results revealed negligible discrepancies between the two beams. Figure 8 demonstrates the minimal differences observed, which were expected due to the similar characteristics of the gamma energy spectra from both beams. This serves as a crucial consistency check for the irradiation process.

6. Conclusions

The preservation of beam properties throughout the entire process, from beam production to gamma generation, is achievable for a better design of gamma-ray irradiators.

The analysis of the RF cavity phase allowed us to observe how the electromagnetic fields within the cavity affect the electron beam. This, in turn, directly influences the gamma beam quality and the efficiency of the irradiation process.

One of the primary studies involved varying the input phase of the beam into the cavity to examine how beam parameters change as a function of this phase. This analysis identified the optimal acceleration region, which is critical for optimizing the performance of the irradiator as the maximum energy spread for the gamma production is at the maximum acceleration gradient.

Setting the RF cavity to produce an electron beam with a mean energy of 6 MeV, the FOM proves useful in setting limits on the design so that the gamma beam can meet quality requirements when necessary, such as in radiotherapy and other scientific applications in medical science.

For applications where only high gamma intensity is required and quality is not an issue, such as water irradiation, the electron to gamma conversion can be improved by designing an RF cavity with higher longitudinal acceptance at the expense of beam quality.

Thanks to the gamma beam similarities, future studies could focus on enhancing irradiation uniformity of the beam produced by the RF cavity and layering through further gamma-ray beam processing in addition to the use of a simple collimation.

Acknowledgments

Part of this work was supported by CONAHCYT (Grants CF-2023-G-1286 and CF-2019/2042). V.M. Lizárraga-Rubio is a doctoral student from Doctorado en Física, Universidad de Guanajuato and received fellowship 923720 from CONAHCYT. J.E. Leyva-Cervantes is a master's student from Maestría en Física, Universidad Autómoma de Sinaloa and received fellowship 1318107 from CONAHCYT.

1. A. Fogliata *et al.*, Definition of parameters for quality assurance of flattening filter free (fff) photon beams in radiation therapy, *Medical Physics* **39** (2012) 6455, https://doi.org/10.1118/1.4754799.
2. A. Zeghari, R. Saaidi, and R. Cherkaoui El Moursli, Enhancement of the dose on 12 mv linac with free flattening filter mode, *Journal of Biomedical Physics and Engineering* **9** (2019) 437, https://doi.org/10.31661/jbpe.v0i0.924.
3. F. Pönisch, U. Titt, O. N. Vassiliev, S. F. Kry, and R.Mohan, Properties of unflattened photon beams shaped by a multileaf collimator, *Medical Physics* **33** (2006) 1738, https://doi.org/10.1118/1.2201149.
4. J. H. Billen and L. M. Young, POISSON SUPERFISH Documentation (LA-UR, 96-1834, 1996).
5. C. S. Technology, Cst, https://www.cst.com/.
6. G. R. Montoya-Soto, B. Yee-Rendon, C. Duarte-Galvan, and C. A. Valerio-Lizarraga, Electromagnetic design and characterization of an s-band 3-cell rf acceleration cavity, *Journal of Physics: Conference Series* **1350** (2019) 012190, https://doi.org/10.1088/1742-6596/1350/1/012190.
7. A. Perrin, J.-F. Amand, T. Muetze, J.-B. Lallement, and S. Lanzone, Travel v4.07 User Manual (2007).
8. C. Valerio-Lizarraga *et al.*, Study of the first mexican rf linear accelerator, *Rev. Mex Fis* **64** (2018) 116, https://doi.org/10.31349/revmexfis.64.116.
9. A. Lichtenberg, Longitudinal phase space transformations, *Nuclear Instruments and Methods* **26** (1964) 243, https://doi.org/10.1016/0029-554X(64)90083-7.
10. J. Besserer *et al.*, An irradiation facility with a vertical beam for radiobiological studies, *Nuclear Instruments and Methods in Physics Research Section A: Accelerators, Spectrometers, Detectors and Associated Equipment* **430** (1999) 154, https://doi.org/10.1016/S0168-9002(99)00195-3.
11. A. Belousov, S. Varzar, and A. Chernyaev, Simulation of the conditions of photon and electron beam irradiation in magnetic fields for increasing conformity of radiation therapy, *Bull. Russ. Acad. Sci. Phys* **71** (2007) 841, https://doi.org/10.3103/S1062873807060172.
12. S. Agostinelli *et al.* (GEANT4), GEANT4-a simulation toolkit, *Nucl. Instrum. Meth. A* **506** (2003) 250, https://doi.org/10.1016/S0168-9002(03)01368-8.
13. F. Stichelbaut, J.-L. Bol, M. Cleland, O. Gréegoire, A. Herer, Y. Jongen, and B. Mullier, The palletron: a high-dose uniformity pallet irradiator with x-rays, *Radiation Physics and Chemistry* **71** (2004) 291, https://doi.org/10.1016/j.radphyschem.2004.03.062.
14. INTERNATIONAL ATOMIC ENERGY AGENCY, Trends in Radiation Sterilization of Health Care Products, Nonserial Publications (International Atomic Energy Agency, Vienna, 2008).
15. C. Srinivas, A primer on theory and operation of linear accelerators in radiation therapy, *Journal of Medical Physics* **44** (2019) 298.
16. L. Manmaker, The Definitive Computer Manual, Chips-R-Us (Silicon Valley, silver ed., 1986).
17. R. Desai and K. M. Rich, Therapeutic role of gamma knife stereotactic radiosurgery in neuro-oncology, *Missouri medicine*, **117** (2020) 33.
18. Z. Zimek, Comparison between EB, gamma, and x-rays facilities for radiation processing (2017) pp. 65.
19. F. Halzen and D. Martin, Quarks and Leptons: an introductory course (Ed. John Wiley, 1984).
20. K. S. Krane, Introductory nuclear physics (Wiley, New York, NY, 1988).